Geophysical Research Letters

Key Points:

- Equivalent porous media can reproduce pressure and temperature evolution at wells but not their distributions within the fractured media
- Consideration of explicit fractures affects stability and induced seismicity in a way that cannot be represented by equivalent media
- Simulating thermo-hydro-mechanical processes requires explicit inclusion of fractures whenever they add inhomogeneities at reservoir scale

Supporting Information:

Supporting Information may be found in the online version of this article.

Correspondence to:

V. Vilarrasa,
victor.vilarrasa@idaea.csic.es

How Equivalent Are Equivalent Porous Media?

Ahmad Zareidarmiyan[1,2,3] ⓘ**, Francesco Parisio**[4] ⓘ**, Roman Y. Makhnenko**[5] ⓘ**, Hossein Salarirad**[1] ⓘ**, and Victor Vilarrasa**[2,3,6] ⓘ

[1]Department of Mining and Metallurgical Engineering, Amirkabir University of Technology—Tehran Polytechnic (AUT), Tehran, Iran, [2]Institute of Environmental Assessment and Water Research (IDAEA), Spanish National Research Council (CSIC), Barcelona, Spain, [3]Associated Unit: Hydrogeology Group UPC-CSIC, Barcelona, Spain, [4]Chair of Soil Mechanics and Foundation Engineering, Freiberg University of Mining and Technology, Freiberg, Germany, [5]Department of Civil and Environmental Engineering, University of Illinois at Urbana-Champaign, Urbana, USA, [6]Mediterranean Institute for Advanced Studies (IMEDEA), Spanish National Research Council (CSIC), Balearic Islands, Spain

Abstract Geoenergy and geoengineering applications usually involve fluid injection into and production from fractured media. Accounting for fractures is important because of the strong poromechanical coupling that ties pore pressure changes and deformation. A possible approach to the problem uses equivalent porous media to reduce the computational cost and model complexity instead of explicitly including fractures in the models. We investigate the validity of this simplification by comparing these two approaches. Simulation results show that pore pressure distribution significantly differs between the two approaches even when both are calibrated to predict identical values at the injection and production wells. Additionally, changes in fracture stability are not well captured with the equivalent porous medium. We conclude that explicitly accounting for fractures in numerical models may be necessary under some circumstances to perform reliable coupled thermohydromechanical simulations, which could be used in conjunction with other tools for induced seismicity forecasting.

Plain Language Summary The subsurface will play an important role in decarbonizing the economy. The transition to carbon neutrality can be accelerated by utilizing geothermal energy, returning carbon underground, and storing energy in the subsurface to offset the fluctuations in production of renewables. These low-carbon geoenergy technologies oftentimes deal with fractured rock masses. To minimize the risks related to geoenergy projects, numerical simulations are performed to predict the response of the subsurface to fluid injection and production. Given the complexity and high computational cost of simulating fractures, fractured rock is usually treated as an equivalent porous medium. Here we investigate the validity of this simplification by comparing these two approaches. We find that even though an equivalent porous medium can reproduce the fluid pressure changes at wells, the pressure distribution within the fractured media significantly differs between the two approaches. Equivalent porous media fail to reliably predict the rock behavior when fracture spacing is within the order of the reservoir size and computer simulations should explicitly include fractures to provide reliable forecasts and reduce the risks of induced seismicity. The latter is necessary to enable a successful deployment of geoenergies to mitigate the climate crisis.

1. Introduction

Fractures are ubiquitous in rock masses and control their transport and deformation properties (Cornet, 2015; Jaeger et al., 2007). On the one hand, fractures represent preferential paths for fluid flow because their permeability is usually several orders of magnitude higher than that of intact rock (Rutqvist, 2015; Witherspoon et al., 1980; Zimmerman & Bodvarsson, 1996). On the other hand, fractures represent weak planes with lower strength and higher deformability than the intact rock (Bandis et al., 1983; Barton, 1976). The hydraulic and mechanical responses of fractured media are strongly coupled, meaning that the deformation induced by pore pressure changes causes permeability changes as a result of fracture opening or closure, which in turn affects the pore pressure (Barton et al., 1985; Stephanson et al., 1997; Tsang, 1999; Watanabe et al., 2012).

Many geoengineering and geoenergy applications, including enhanced geothermal systems, geologic carbon storage, energy storage, and nuclear waste disposal, take place in fractured media (Rutqvist & Stephansson, 2003) where they induce pore pressure, temperature, and stress changes that are mostly controlled by the physical properties and topology of the fractures. Moreover, the presence of fractures introduces additional nonlinearity and discontinuities in the displacement field. The combined effect of pressure and stress changes affects fracture stability and may induce seismicity (Clarke et al., 2014; Ellsworth et al., 2019; Häring et al., 2008; National Research Council, 2013). The magnitude of induced seismicity is proportional to the rupture area and its frequency distribution obeys a power law called the Gutenberg-Richter law (Kanamori & Brodsky, 2004).

Including fractures in numerical thermohydromechanical (THM) models is possible and several approaches have been proposed (e.g., Keilegavlen et al., 2021; Pan et al., 2014; T. Wang et al., 2019; Yao et al., 2018; Zareidarmiyan, Salarirad, et al., 2020). Yet, explicitly accounting for fractures in numerical models of poromechanical problems is a challenging task and often comes at the expenses of a very high computational cost (Lei et al., 2017; McDermott & Kolditz, 2006; Pandey et al., 2017; Salimzadeh et al., 2018; Thomas et al., 2020; Yoshioka et al., 2019). In order to facilitate the calculation for large problems, dense fractured networks are often simplified as equivalent porous media, like the ubiquitous joint model, and computational resources are used for other purposes, such as reactive transport, phase changes, and dynamics or complex plasticity models (e.g., Birdsell et al., 2018; Liu et al., 2009; Parisio, Vilarrasa, et al., 2019; Rinaldi et al., 2015; Rutqvist, Wu, et al., 2002; Rutqvist et al., 2005; Taron & Elsworth, 2009; Vallier et al., 2020; Y. Wang et al., 2019).

Here, we investigate the validity of this simplification made by representing a naturally fractured reservoir with an equivalent porous medium. We compare the pore pressure, temperature, and stress changes caused by injection of cold water and production from a distant well between a model that explicitly includes fractures and one that implicitly includes them as an equivalent porous medium. In particular, we assess the induced seismicity potential resulting from both approaches. As a case study, we use the data from Hontomin Technology Development Plant (TDP) for CO_2 geological storage. The storage formation at Hontomin is a fractured carbonate rock with a very low-permeable rock matrix and two perpendicular dominant fracture sets (de Dios et al., 2017). We investigate the validity of equivalent porous media to reproduce the fluid flow and geomechanical response to injection and production into a fractured reservoir.

2. Materials and Methods

2.1. Geometry

We adopt a plane strain geometry for the Hontomin TDP site. The model consists of three horizontal layers that represent the caprock, the reservoir, and the bedrock with thickness of 160, 120, and 50 m, respectively. The reservoir is a fractured carbonate with two perpendicular fracture sets, one subhorizontal and the other one subvertical (de Dios et al., 2017). We represent the two sets with 10-cm thick planar fractures embedded into the reservoir layer dipping 15° and 75°. Water is injected into the reservoir through a horizontal well on the left-hand side of the model and produced from another horizontal well on the right-hand side of the model. The two wells are horizontally spaced by 500 m and a mass flow rate of $\pm 5 \cdot 10^{-3}$ kg/s/m is applied (Figure S1). In addition to the fractured reservoir model, we model an equivalent porous medium that yields the same injection pressure in the long term after calibrating the equivalent permeability.

2.2. THM Model

Nonisothermal fluid flow in deformable geologic media requires solving the equations of mass, energy, and momentum conservation. Neglecting the inertial term, that is, quasistatic condition, the momentum balance results in:

$$\nabla \cdot \boldsymbol{\sigma} + \mathbf{b} = 0, \tag{1}$$

where $\boldsymbol{\sigma}\left(ML^{-1}T^{-2}\right)$ is the total stress tensor and $\mathbf{b}\left(ML^{-2}T^{-2}\right)$ is the body forces vector. Fluid mass conservation can be expressed as (Bear, 1972)

$$\frac{\partial(\phi\rho)}{\partial t} + \nabla.(\mathbf{q}\rho) = r, \tag{2}$$

where $\phi\left(L^3 L^{-3}\right)$ is the porosity, $t(\mathrm{T})$ is the time, $\rho\left(ML^{-3}\right)$ is the fluid density, $\mathbf{q}(L^3 L^{-2} T^{-1})$ is the volumetric flux, and $r(ML^{-3}T)$ is the source/sink term of fluid. The volumetric flux is calculated using Darcy's law as

$$\mathbf{q} = -\frac{k}{\eta}(\nabla p + \rho g \nabla z), \tag{3}$$

where $k(L^2)$ is the intrinsic permeability, $\eta\left(ML^{-1}T^{-1}\right)$ is the dynamic viscosity, $p(ML^{-1}T^{-2})$ is the fluid pressure, $g(LT^{-2})$ is the acceleration of gravity, and $z[L]$ is the elevation from a reference plane.

Energy balance is given by (Nield & Bejan, 2006)

$$\frac{\partial\left((1-\phi)\rho_s h_s + \phi\rho h\right)}{\partial t} + \nabla.\left(-\lambda\nabla T + \rho h\mathbf{q}\right) = 0, \tag{4}$$

where $\rho_s\left(ML^{-3}\right)$ is the solid phase density, $h_s\left(L^2 T^{-2}\right)$ is the solid phase enthalpy, $h\left(L^2 T^{-2}\right)$ is the fluid phase enthalpy, $\lambda\left(MLT^{-3}\Theta\right)$ is thermal conductivity of the geological medium, and $T\left(\Theta\right)$ is temperature. We assume thermal equilibrium of all phases at every point.

We consider the linear thermoporoelasticity theory in porous media to account for the effect of pore pressure and temperature changes on rock deformation. Elastic strain tensor $\boldsymbol{\varepsilon}\left(LL^{-1}\right)$ depends on the total stress, overpressure, and temperature as

$$\boldsymbol{\varepsilon} = \frac{1+\nu}{E}\boldsymbol{\sigma} - \frac{3\nu}{E}\sigma_m\mathbf{I} - \frac{1-2\nu}{E}\left(\alpha\Delta p\mathbf{I}\right) - \Delta T\alpha_T\mathbf{I}, \tag{5}$$

where $\sigma_m = \left(tr(\boldsymbol{\sigma})/3\right)\left(ML^{-1}T^{-2}\right)$ is the mean total stress, $\mathbf{I}$ (-) is the identity matrix, $\alpha_T\left(\Theta^{-1}\right)$ is the linear thermal expansion coefficient, $\nu(-)$ and $E(ML^{-1}T^{-2})$ are the drained Poisson's ratio and the Young's modulus of the rock, respectively, and $\alpha\left(-\right)$ is the Biot coefficient. The effective stress tensor is $\boldsymbol{\sigma}' = \boldsymbol{\sigma} - \alpha p\mathbf{I}$.

Fractures are modeled using a finite thickness representation with a higher permeability and lower normal and shear stiffness than the surrounding rock matrix (Zareidarmiyan, Salarirad et al., 2020). For the sake of comparing the fractured media and the equivalent porous medium, we consider that fracture permeability remains constant throughout the whole simulation. Otherwise, an equivalent porous medium cannot be obtained. We assume linear thermoelastic behavior up to failure (and subsequent induced microseismicity) described by the Mohr-Coulomb failure criterion (Labuz & Zang, 2012)

$$\tau_n = c + \mu\sigma'_n, \tag{6}$$

where $\tau_n\left(ML^{-1}T^{-2}\right)$ and $\sigma'_n\left(ML^{-1}T^{-2}\right)$ are, respectively, the shear stress and the effective normal stress acting on a plane of a given orientation, $c(ML^{-1}T^{-2})$ is cohesion, and $\mu\left(-\right)$ is the friction coefficient, which is expressed in terms of the friction angle as $\mu = \tan\varphi$. Theoretically, the effective stress for failure analyses is the Terzaghi effective stress, that is, with Biot coefficient equal to one (Makhnenko & Labuz, 2015). Because the assumption of $\alpha = 1$ has been made for all rocks (Table S1), the adopted formulation is consistent and does not need to differentiate between the two possible effective stress choices. Considering cohesionless fractures, the mobilized friction coefficient can be defined as the ratio of the shear stress to the effective normal stress

$$\mu_{\mathrm{mob}} = \frac{\tau_n}{\sigma'_n} \tag{7}$$

The mobilized friction coefficient quantifies the shear slip tendency and how close the stress state is to shear failure conditions. Shear failure occurs when the mobilized friction coefficient is equal to the actual friction coefficient. As an alternative representation that does not imply a specific orientation in space, one can express the mobilized friction resistance in terms of invariants of the effective stress tensor σ'_{ij}. Considering the mean effective stress $\sigma'_m = tr\left(\sigma'_{ij}\right)/3$ and the deviatoric stress $\sigma_D = \sqrt{3\left(\sigma'_{ij}\sigma'_{ij}\right)/2}$, the mobilized friction angle in a normal faulting stress regime can be expressed as

$$\phi_{\mathrm{mob}} = \arcsin\left(\frac{3M}{6+M}\right),\tag{8}$$

where $M = \sigma_D/\sigma'_m$.

2.3. Numerical Models

The model represents a two-dimensioanl plane strain vertical section of the formation. Initial conditions correspond to a hydrostatic pore pressure with 15 MPa at the center of the reservoir, a geothermal gradient that yields a temperature of 45°C in the reservoir at a depth of 1.44 km, and a normal faulting stress regime, with the horizontal to vertical effective stress ratio being equal to 0.65, that is, $\sigma'_h = 0.65\sigma'_v$. Tables S1 and S2 show the material and fluid properties used in the simulations of the fractured reservoir. For the equivalent porous medium, permeability has been set at $2.75 \cdot 10^{-16}$ m^2 and the rest of the properties are equal to those of the rock matrix.

The mechanical boundary conditions are the lithostatic stress on the upper boundary, no displacement perpendicular to the lateral boundaries, and fixed displacement on the lower boundary. The hydraulic boundary conditions are no flow on all boundaries except from the wells where water is injected or produced at a prescribed flow rate of 5.10^{-3} kg/s/m for 30 years. The wells maintain their location in the equivalent porous medium model. We solve the problem both in isothermal conditions and considering an injection temperature being 20°C colder than that of the reservoir.

An unstructured mesh with 17,775 quadrilateral elements is used. The mesh is refined around fractures, especially at fracture intersections. For the equivalent porous medium, we have used the same mesh as for the fractured reservoir and a more homogeneous mesh with refinement around the wells, obtaining the same results in both cases. Simulations are performed with CODE_BRIGHT (Olivella et al., 1996), an extensively validated finite element numerical code that solves coupled THM problems in porous media. The models are available at Zareidarmiyan, Parisio, et al. (2020).

2.4. Material Properties

The reservoir rock properties are taken from the measurements performed on limestone Sopeña Formation from Hontomin injection well (de Dios et al., 2017). The physical properties of Sopeña Formation are highly heterogeneous and the fluctuations are likely connected to the presence of fractures in some of the tested specimens, that is, porosity measurements oscillate from 0.002 to 0.16. In the numerical analyses, we assumed mean values for the elastic and strength properties (Table S1). The permeability of the rock matrix is reported to be $\sim10^{-18}$ m^2, while for the fractures it can go up to $\sim10^{-13}$ m^2. Marly Lias constitutes the caprock (permeability $<10^{-18}$ m^2) at Hontomin and given the lack of information, we have assumed Opalinus Clay as an analogue for the physical properties of the ductile caprock and base rock. Opalinus Clay is a low-permeable Jurassic shale from northern Switzerland with high CO_2 entry pressure values (Makhnenko et al., 2017). Undrained poroelastic parameters and permeability perpendicular to the bedding planes are measured for the fully saturated shale (Makhnenko & Podladchikov, 2018) and are included in the model. Failure properties of shale are adopted from the literature (Gräsle, 2011).
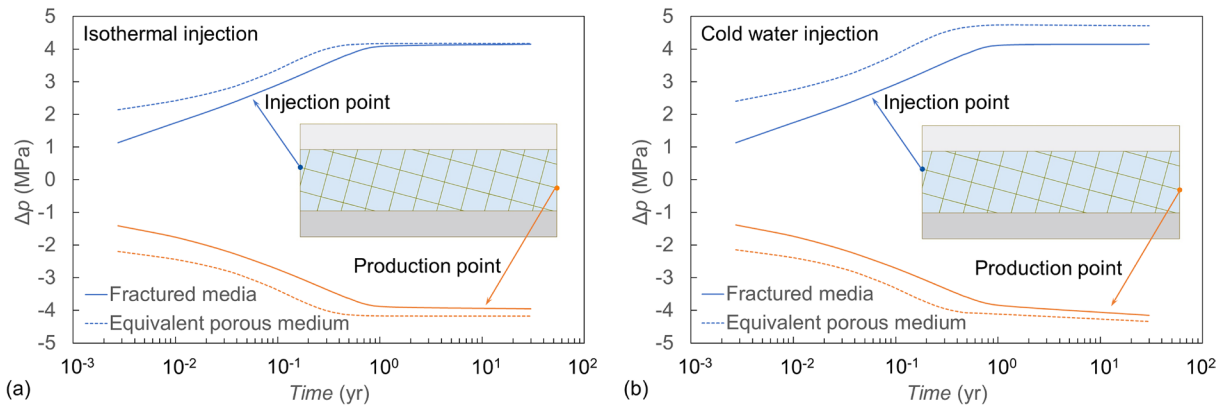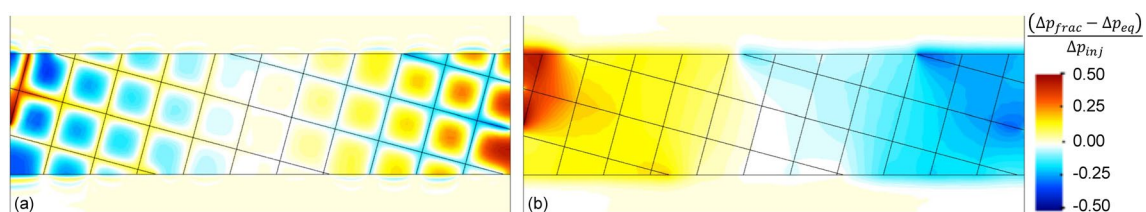
Figure 1. Pressure change evolution at the injection and production points considering a fractured reservoir and an equivalent porous medium for (a) isothermal conditions and (b) injection of cold water.

3. Results

The pressure change Δp is positive or negative at the injection or production wellbore, respectively (Figure 1). The steady-state conditions in isothermal injection yield the same pressure buildup at the injection well for both the fractured and the equivalent porous medium, although a slight difference is observed at the production highlighting that flow through fractures differs from that of an equivalent porous medium (Figure 1a). The rate of pressure change is more rapid for the equivalent porous medium, which reaches steady-state conditions within approximately 6 months, while it takes around 1 yr for the fractured medium because of the higher diffusion time across the low-permeable matrix blocks. The injection overpressure difference between equivalent and fractured medium is greater when cold fluid is injected (Figure 1b) because the effect of the increase in fluid viscosity (Equation S2) on pressure buildup is smaller in the fractured medium as a result of the localized preferential flow paths in comparison to the distributed head losses in the equivalent porous medium. At the production well, the pressure change has not reached a steady-state condition after 30 yrs of injection (Figure 1b) due to the continuously propagating cooling front. The thermal diffusion process in fractured rock, which includes conduction and advection, takes longer time than the pore pressure diffusion.

In all cases, the difference between equivalent and fractured medium is small (by design) at the injection and production wells and the equivalent approach does a consistent job in approximating fractures. However, the spatial distribution of pore pressure within the reservoir significantly differs between the fractured medium and the equivalent porous medium (Figures S2 and S3). The difference between the two approaches is as high as 50% when normalized with respect to the pressure change occurring at the injection well, which is the largest pressure change within the reservoir (Figure 2). The difference in pore pressure distribution between the fractured and equivalent approach is concentrated around the fractures during early time of the simulation because pressure has not completely diffused through the matrix blocks (Figures 2a and S2). In contrast, pore pressure diffusion has a smearing effect in the long term, as the difference is more continuously distributed in space and does not conform with the fracture topology, but caused by the fact

Figure 2. Pressure change difference between the fractured reservoir, Δp_{frac}, and the equivalent porous medium, Δp_{eq}, normalized with respect to the pressure difference at the injection well, Δp_{inj}, in (a) early times (30 days of operation) and (b) late times (30 years of operation).
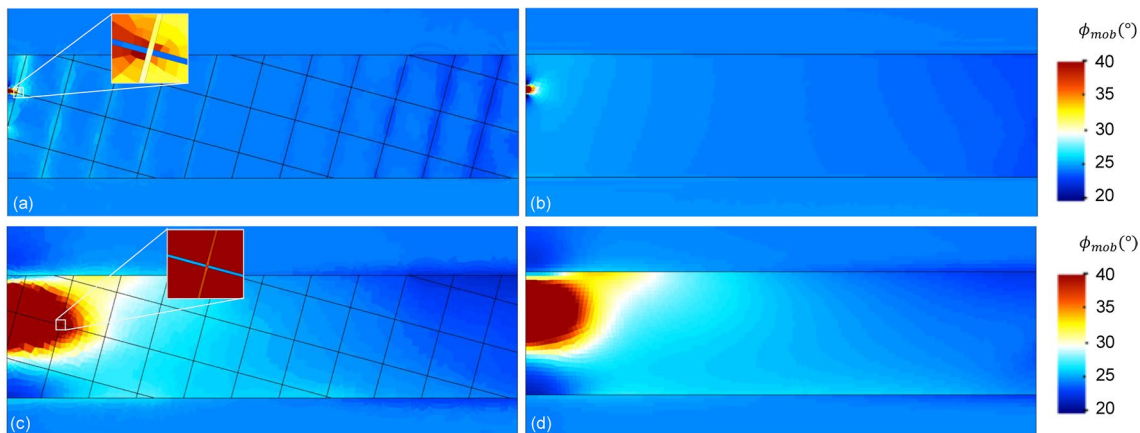
Figure 3. Mobilized friction angle development due to cold water injection at early times (30 days) for (a) The fractured reservoir and (b) The equivalent porous medium, and at late times (30 years) for (c) The fractured reservoir and (d) The equivalent porous medium.

that the pressure gradient is lower along fractures and is distributed over a longer distance than through the equivalent porous medium (Figures 2b and S2).

The late-time (30 years of operation) mobilized friction angle has a similar space distribution for the equivalent and fractured media approaches (Figures 3c and 3d). For cold water injection, assuming a friction angle of 30°, resistance is exceeded at the injection wellbore because of pressure buildup and cooling. The region undergoing failure is entirely localized within the injection formation, although a portion of the interface between the aquifer and the caprock is exceeding frictional resistance in both cases. The smeared nature of the equivalent porous medium approach does not distinguish between critically and noncritically oriented fractures (Figures 3b and 3d). On the contrary, the enhanced information of the fractured medium approach shows that the mobilized friction angle along subvertical fractures is exceeding resistance, whereas the subhorizontal fracture set remains stable (inset Figures 3a and 3c).

The differences between the two approaches in terms of fracture stability can be highlighted by plotting the mobilized friction coefficient in all the considered cases and along fractures A, B, and C (Figure 4). Fracture A is connected to the injection wellbore and, at isothermal conditions, the mobilized friction coefficient is the highest closer to the wellbore in the equivalent porous medium, while it becomes smaller than one of the fractured mediums at greater distances (Figure 4a). Cold fluid injection causes the increase in the mobilized friction coefficient in both media, with values in the equivalent medium potentially exceeding failure, while they never exceed the threshold of $\mu = 0.6$ in the fractured medium (Figure 4d). Note that fracture A is a subhorizontal fracture, thus it is not critically oriented in a normal faulting stress regime like the one considered in this study. Contrary to fracture A, fracture B is close to the critical orientation (Figures 4b and 4e) and the mobilized friction coefficient after injection is higher for the fractured medium. In this case, the mobilized friction coefficient remains below failure threshold for the isothermal injection (Figure 4b), while the cooling effect reduces the mean effective stress and mobilized friction coefficient has a sharp increment over large patches. Fluid production has a beneficial effect because the pressure reduction with time stabilizes fracture C (Figure 4c), with a more pronounced effect in the fractured medium. An inversion is observed between short- and long-time behavior during cold injection and mobilized friction coefficient slightly increases close to the production point (Figure 4f). Nevertheless, no failure occurs and the mobilized friction coefficient in the noncritically oriented fracture C never exceeds failure conditions.

4. Discussion

Equivalent porous media can misleadingly reproduce the pore pressure evolution measured at lower-dimensionality observation points of a fractured medium as a result of injection or production (Figures 1 and 2). Even though an equivalent porous medium can be used to reproduce fluid flow through fractured media under certain conditions, like for densely fractured media (Long et al., 1982; Scanlon et al., 2003), our simulations show that the pressure distribution within the fractured medium can differ as much as 50%
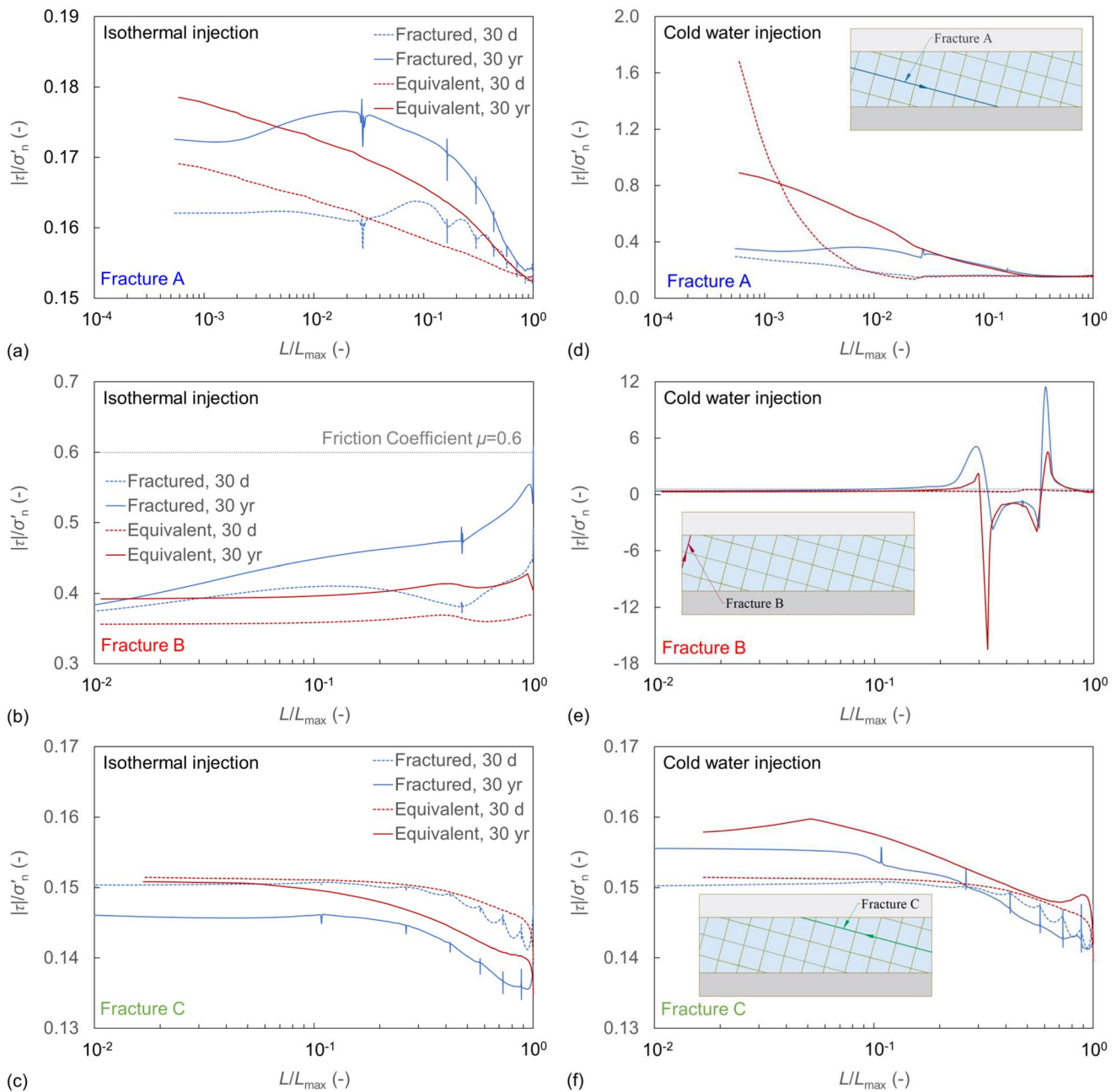
Figure 4. Mobilized friction coefficient, that is, deviatoric stress to effective normal stress ratio, along fractures A, B, and C for early times (30 days) and late times (30 yrs) for isothermal conditions (a)–(c) and injection of cold water (d)–(f) when considering a fractured reservoir and an equivalent porous medium.

of the pressure change undergone at the wells. Such difference occurs both in the short term, when pore pressure has not completely diffused through the rock matrix, and in the long term, when pore pressure diffusion has already occurred. As a result, heat transport also differs between an equivalent porous medium and the fractured medium.

Fractures are usually more permeable and consequently heat advection dominates along fractures, whereas heat conduction prevails within the matrix: The temperature change is larger along fractures in the fractured medium compared to the one in the matrix in the equivalent porous medium (Figure S4 and S5). The temperature changes are restricted to a small rock volume around the injection well because of the lower thermal diffusivity compared to the hydraulic diffusivity (De Simone et al., 2017). The differences in the

pore pressure and temperature distributions highlight the limitations of the equivalent porous media to accurately reproduce fluid flow and heat transport within a fractured rock.

It should be noted that we have neglected the effect of changes in fracture aperture on their permeability. Including this characteristic, that is, permeability enhancement due to fracture opening when inertial losses become negligible (Rutqvist, 2015; Zhou et al., 2019), would have significantly increased the differences in pore pressure (Birdsell et al., 2018) and temperature distribution between the fractured and the equivalent porous medium. Furthermore, due to the nonlinearity of the problem, an equivalent permeability that reflects the pore pressure evolution at the injection and production wells would not be possible to reproduce.

Induced (micro) seismicity assessment is significantly affected by the differences in the pore pressure and temperature distributions, even when considering constant fracture permeability (Figure 4). In addition to the potential local stress variations around fractures previous to injection/production (Gao et al., 2019; Lei & Gao, 2018), pore pressure and temperature changes induce local rotation of the principal stress tensor along fractures that can be reproduced only when fractures are explicitly included in the model (De Simone et al., 2013; Zareidarmiyan et al., 2018, Zareidarmiyan, Salarirad, et al., 2020). The lower stiffness of fractures compared to the rock matrix (Pyrak-Nolte & Morris, 2000) generates a lower cooling-induced stress reduction and affects both the induced poro and thermomechanical stresses and thus, fracture stability.

Measurements of the physical properties of intact and fractured rock in the lab at representative pressure and temperature provide fundamental insights on multiphysical processes but are difficult to perform (Braun et al., 2020; Faoro et al., 2009; Samuelson et al., 2009). Additionally, fractures introduce a length-scale dependency and lab-sized results must be properly upscaled to reservoir conditions (Parisio, Tarokh, et al., 2019). In this regard, recent experiments at intermediate scale with comprehensive monitoring systems can provide insight on behavior of decameter-long fractures and bridge various scales (Amann et al., 2018; Guglielmi et al., 2020). Fluid-solid interactions and chemical reactions also play an important role and in the case of CO_2 injection can significantly change fracture properties (Pluymakers et al., 2014), and the additional effects on induced seismicity are to be further studied in the lab (Elsworth & Yasuhara, 2006; Li et al., 2007; Samuelson & Spiers, 2012).

Numerical modeling of fractured media also possesses some challenges. Computationally, at the characteristic length scale of many reservoir applications, the fracture density can become excessively high and including all the discontinuities in numerical models may become unfeasible. Homogenization and other upscaling techniques are often the only solution for overcoming this issue (Bonnet et al., 2001; Gan & Elsworth, 2016; Lei et al., 2015). However, our numerical simulation results show that the information loss from neglecting the explicit representation of fractures at a spacing that is in the order of the reservoir's size can lead to unacceptable approximation on stability.

The choice of using either the fractured or equivalent media approach should be carefully pondered on a case-by-case basis and should heavily rely on available structural geology information. At very high fracture density, the equivalent approach and other homogenization-based schemes would be more convenient and, assuming the rock mass representative elementary volume to contain enough fractures, potentially almost no information would be lost. Modeling bedding planes in shale, which are tightly spaced discontinuities that result in overall anisotropy, is an example where continuous approaches (Parisio et al., 2018) yield similar predictions to high-resolution discrete ones (Lisjak et al., 2015; Kim et al., 2020). Multiscale methods have the potential to bridge the gap between the explicit fracture modeling and equivalent continuum approaches and, along with machine learning and data-driven computational schemes, could resolve the large spatial scale separation typical of fractured reservoirs (Wang & Sun, 2018). Nevertheless, the high computational costs required from modeling explicit fractured media must be justified by a proper knowledge about the characteristics of the subsurface fracture network. Otherwise, a high uncertainty on the fracture network geometry and characteristics hinders the effort of highly realistic models.

5. Conclusions

We consider a problem of fluid injection and production from a fractured reservoir and compare pore pressure and temperature distributions between a fractured medium and its equivalent porous medium and how they affect fracture stability. An equivalent porous medium that reproduces the pressure evolution at the injection and production wells can be obtained, provided that fracture permeability remains constant. However, the pore pressure distribution significantly differs between the two approaches as a result of the higher permeability of fractures. Differences are also evident when evaluating fracture stability. Therefore, achieving an accurate simulation of the THM processes occurring in fractured media requires explicitly including fractures in the reservoir models whenever they introduce inhomogeneities at the reservoir scale.

Data Availability Statement

The input files of the simulations used in this manuscript are available at the institutional repository Digital. CSIC, which practices FAIR principles: https://digital.csic.es/handle/10261/212935

References

Amann, F., Gischig, V., Evans, K., Doetsch, J., Jalali, R., Valley, B., et al. (2018). The seismo-hydromechanical behavior during deep geothermal reservoir stimulations: Open questions tackled in a decameter-scale in situ stimulation experiment. *Solid Earth*, *9*, 115–137. https://doi.org/10.5194/se-9-115-2018

Bandis, S. C., Lumsden, A. C., & Barton, N. R. (1983). Fundamentals of rock joint deformation. *International Journal of Rock Mechanics and Mining Sciences & Geomechanics Abstracts*, *20*(6), 249–268. https://doi.org/10.1016/0148-9062(83)90595-8

Barton, N. (1976). The shear strength of rock and rock joints. *International Journal of Rock Mechanics and Mining Sciences & Geomechanics Abstracts*, *13*(9), 255–279. https://doi.org/10.1016/0148-9062(76)90003-6

Barton, N., Bandis, S., & Bakhtar, K. (1985). Strength, deformation and conductivity coupling of rock joints. In *International Journal of Rock Mechanics and Mining Sciences & Geomechanics Abstracts* (Vol. 22, pp. 121–140). Pergamon. https://doi.org/10.1016/0148-9062(85)93227-9

Bear, J. (1972). *Dynamics of fluids in porous media*. Elsevier.

Birdsell, D. T., Karra, S., & Rajaram, H. (2018). Code development for modeling induced seismicity with flow and mechanics using a discrete fracture network and matrix formulation with evolving hydraulic diffusivity. Paper presented at *2nd International Discrete Fracture Network Engineering Conference*. Seattle, WA. (DFNE 18-565).

Bonnet, E., Bour, O., Odling, N. E., Davy, P., Main, I., Cowie, P., & Berkowitz, B. (2001). Scaling of fracture systems in geological media. *Reviews of Geophysics*, *39*(3), 347–383. https://doi.org/10.1029/1999rg000074

Braun, P., Ghabezloo, S., Delage, P., Sulem, J., & Conil, N. (2020). Thermo-poro-elastic behaviour of a transversely isotropic shale: Thermal expansion and pressurization. *Rock Mechanics and Rock Engineering*, *54*(1), 359–375.

Clarke, H., Eisner, L., Styles, P., & Turner, P. (2014). Felt seismicity associated with shale gas hydraulic fracturing: The first documented example in Europe. *Geophysical Research Letters*, *41*(23), 8308–8314. https://doi.org/10.1002/2014gl062047

Cornet, F. (2015). *Elements of crustal geomechanics*. Cambridge University Press. https://doi.org/10.1017/cbo9781139034050

de Dios, J. C., Delgado, M. A., Martínez, C., Ramos, A., Álvarez, I., Marín, J. A., & Salvador, I. (2017). Hydraulic characterization of fractured carbonates for CO$_2$ geological storage: Experiences and lessons learned in Hontomín Technology Development Plant. *International Journal of Greenhouse Gas Control*, *58*, 185–200. https://doi.org/10.1016/j.ijggc.2017.01.008

De Simone, S., Carrera, J., & Vilarrasa, V. (2017). Superposition approach to understand triggering mechanisms of post-injection induced seismicity. *Geothermics*, *70*, 85–97. https://doi.org/10.1016/j.geothermics.2017.05.011

De Simone, S., Vilarrasa, V., Carrera, J., Alcolea, A., & Meier, P. (2013). Thermal coupling may control mechanical stability of geothermal reservoirs during cold water injection. *Physics and Chemistry of the Earth, Parts A/B/C*, *64*, 117–126. https://doi.org/10.1016/j.pce.2013.01.001

Ellsworth, W. L., Giardini, D., Townend, J., Ge, S., & Shimamoto, T. (2019). Triggering of the Pohang, Korea, Earthquake (Mw 5.5) by enhanced geothermal system stimulation. *Seismological Research Letters*, *90*(5), 1844–1858.

Elsworth, D., & Yasuhara, H. (2006). Short-timescale chemo-mechanical effects and their influence on the transport properties of fractured rock. *Pure and Applied Geophysics*, *163*, 2051–2070. https://doi.org/10.1007/s00024-006-0113-3

Faoro, I., Niemeijer, A., Marone, C., & Elsworth, D. (2009). Influence of shear and deviatoric stress on the evolution of permeability in fractured rock. *Journal of Geophysical Research*, *114*, B01201. https://doi.org/10.1029/2007jb005372

Gan, Q., & Elsworth, D. (2016). A continuum model for coupled stress and fluid flow in discrete fracture networks. *Geomechanics and Geophysics for Geo-Energy and Geo-Resources*, *2*(1), 43–61. https://doi.org/10.1007/s40948-015-0020-0

Gao, K., Lei, Q., Bozorgzadeh, N., & Chau, V. (2019). Can we estimate far-field stress using the mean of local stresses? An examination based on numerical simulations. *Computers and Geotechnics*, *116*, 103188. https://doi.org/10.1016/j.compgeo.2019.103188

Gräsle, W. (2011). Multistep triaxial strength tests: Investigating strength parameters and pore pressure effects on Opalinus clay. *Physics and Chemistry of the Earth, Parts A/B/C*, *36*, 1898–1904. https://doi.org/10.1016/j.pce.2011.07.024

Guglielmi, Y., Nussbaum, C., Jeanne, P., Rutqvist, J., Cappa, F., & Birkholzer, J. (2020). Complexity of fault rupture and fluid leakage in shale: Insights from a controlled fault activation experiment. *Journal of Geophysical Research: Solid Earth*, *125*(2), e2019JB017781. https://doi.org/10.1029/2019jb017781

Häring, M. O., Schanz, U., Ladner, F., & Dyer, B. C. (2008). Characterisation of the basel 1 enhanced geothermal system. *Geothermics*, *37*(5), 469–495. https://doi.org/10.1016/j.geothermics.2008.06.002

Jaeger, J. C., Cook, N. G., & Zimmerman, R. (2007). *Fundamentals of rock mechanics*. John Wiley & Sons.

Kanamori, H., & Brodsky, E. E. (2004). The physics of earthquakes. *Reports on Progress in Physics*, *67*(8), 1429–1496. https://doi.org/10.1088/0034-4885/67/8/r03

Keilegavlen, E., Berge, R., Fumagalli, A., Starnoni, M., Stefansson, I., Varela, J., & Berre, I. (2021). Porepy: An open-source software for simulation of multiphysics processes in fractured porous media. *Computers and Geosciences*, *25*(1), 243–265. https://doi.org/10.1007/s10596-020-10002-5

Kim, K., Rutqvist, J., & Birkholzer, J. (2020). Lattice modeling of excavation damage in argillaceous clay formations: Influence of deformation and strength anisotropy. *Tunnelling and Underground Space Technology*, *98*, 103196. https://doi.org/10.1016/j.tust.2019.103196

Labuz, J. F., & Zang, A. (2012). Mohr-Coulomb failure criterion. *Rock Mechanics and Rock Engineering*, *45*(6), 975–979. https://doi.org/10.1007/s00603-012-0281-7

Lei, Q., & Gao, K. (2018). Correlation between fracture network properties and stress variability in geological media. *Geophysical Research Letters*, *45*(9), 3994–4006. https://doi.org/10.1002/2018gl077548

Lei, Q., Latham, J.-P., & Tsang, C.-F. (2017). The use of discrete fracture networks for modelling coupled geomechanical and hydrological behaviour of fractured rocks. *Computers and Geotechnics*, *85*, 151–176. https://doi.org/10.1016/j.compgeo.2016.12.024

Lei, Q., Latham, J.-P., Tsang, C.-F., Xiang, J., & Lang, P. (2015). A new approach to upscaling fracture network models while preserving geostatistical and geomechanical characteristics. *Journal of Geophysical Research: Solid Earth*, *120*(7), 4784–4807. https://doi.org/10.1002/2014jb011736

Li, Q., Wu, Z., Lei, X.-L., Murakami, Y., & Satoh, T. (2007). Experimental and numerical study on the fracture of rocks during injection of CO_2-saturated water. *Environmental Geology*, *51*, 1157–1164. https://doi.org/10.1007/s00254-006-0406-y

Lisjak, A., Garitte, B., Grasselli, G., Müller, H. R., & Vietor, T. (2015). The excavation of a circular tunnel in a bedded argillaceous rock (Opalinus Clay): Short-term rock mass response and FDEM numerical analysis. *Tunnelling and Underground Space Technology*, *45*, 227–248. https://doi.org/10.1016/j.tust.2014.09.014

Liu, H.-H., Rutqvist, J., & Berryman, J. G. (2009). On the relationship between stress and elastic strain for porous and fractured rock. *International Journal of Rock Mechanics and Mining Sciences*, *46*(2), 289–296. https://doi.org/10.1016/j.ijrmms.2008.04.005

Long, J. C. S., Remer, J. S., Wilson, C. R., & Witherspoon, P. A. (1982). Porous media equivalents for networks of discontinuous fractures. *Water Resources Research*, *18*(3), 645–658. https://doi.org/10.1029/wr018i003p00645

Makhnenko, R. Y., & Labuz, J. F. (2015). Dilatant hardening of fluid-saturated sandstone. *Journal of Geophysical Research: Solid Earth*, *120*(2), 909–922. https://doi.org/10.1002/2014jb011287

Makhnenko, R. Y., & Podladchikov, Y. Y. (2018). Experimental poroviscoelasticity of common sedimentary rocks. *Journal of Geophysical Research: Solid Earth*, *123*, 7586–7603. https://doi.org/10.1029/2018jb015685

Makhnenko, R. Y., Vilarrasa, V., Mylnikov, D., & Laloui, L. (2017). Hydromechanical aspects of CO_2 breakthrough into clay-rich caprock. *Energy Procedia*, *114*, 3219–3228. https://doi.org/10.1016/j.egypro.2017.03.1453

McDermott, C., & Kolditz, O. (2006). Geomechanical model for fracture deformation under hydraulic, mechanical and thermal loads. *Hydrogeology Journal*, *14*(4), 485–498. https://doi.org/10.1007/s10040-005-0455-4

National Research Council. (2013). *Induced seismicity potential in energy technologies*. National Academies Press.

Nield, D. A., & Bejan, A. (2006). *Convection in porous media*. Springer.

Olivella, S., Gens, A., Carrera, J., & Alonso, E. E. (1996). Numerical formulation for a simulator (CODE_BRIGHT) for the coupled analysis of saline media. *Engineering Computations*, *13*(7), 87–112. https://doi.org/10.1108/02644409610151575

Pan, P.-Z., Rutqvist, J., Feng, X.-T., & Yan, F. (2014). TOUGH-RDCA modeling of multiple fracture interactions in caprock during CO_2 injection into a deep brine aquifer. *Computers & Geosciences*, *65*, 24–36. https://doi.org/10.1016/j.cageo.2013.09.005

Pandey, S. N., Chaudhuri, A., & Kelkar, S. (2017). A coupled thermo-hydro-mechanical modeling of fracture aperture alteration and reservoir deformation during heat extraction from a geothermal reservoir. *Geothermics*, *65*, 17–31. https://doi.org/10.1016/j.geothermics.2016.08.006

Parisio, F., Tarokh, A., Makhnenko, R., Naumov, D., Miao, X.-Y., Kolditz, O., & Nagel, T. (2019). Experimental characterization and numerical modelling of fracture processes in granite. *International Journal of Solids and Structures*, *163*, 102–116. https://doi.org/10.1016/j.ijsolstr.2018.12.019

Parisio, F., Vilarrasa, V., & Laloui, L. (2018). Hydro-mechanical modeling of tunnel excavation in anisotropic shale with coupled damage-plasticity and micro-dilatant regularization. *Rock Mechanics and Rock Engineering*, *51*(12), 3819–3833. https://doi.org/10.1007/s00603-018-1569-z

Parisio, F., Vilarrasa, V., Wang, W., Kolditz, O., & Nagel, T. (2019). The risks of long-term re-injection in supercritical geothermal systems. *Nature Communications*, *10*(1), 1–11. https://doi.org/10.1038/s41467-019-12146-0

Pluymakers, A. M. H., Samuelson, J. E., Niemeijer, A. R., & Spiers, C. J. (2014). Effects of temperature and CO_2 on the frictional behavior of simulated anhydrite fault rock. *Journal of Geophysical Research: Solid Earth*, *119*, 8728–8747. https://doi.org/10.1002/2014jb011575

Pyrak-Nolte, L. J., & Morris, J. P. (2000). Single fractures under normal stress: The relation between fracture specific stiffness and fluid flow. *International Journal of Rock Mechanics and Mining Sciences*, *37*(1–2), 245–262. https://doi.org/10.1016/s1365-1609(99)00104-5

Rinaldi, A. P., Rutqvist, J., Sonnenthal, E. L., & Cladouhos, T. T. (2015). Coupled THM modeling of hydroshearing stimulation in tight fractured volcanic rock. *Transport in Porous Media*, *108*(1), 131–150. https://doi.org/10.1007/s11242-014-0296-5

Rutqvist, J. (2015). Fractured rock stress-permeability relationships from in situ data and effects of temperature and chemical-mechanical couplings. *Geofluids*, *15*(1–2), 48–66. https://doi.org/10.1111/gfl.12089

Rutqvist, J., Barr, D., Datta, R., Gens, A., Millard, A., Olivella, S., et al. (2005). Coupled thermal–hydrological–mechanical analyses of the Yucca mountain drift scale test—Comparison of field measurements to predictions of four different numerical models. *International Journal of Rock Mechanics and Mining Sciences*, *42*(5–6), 680–697. https://doi.org/10.1016/j.ijrmms.2005.03.008

Rutqvist, J., & Stephansson, O. (2003). The role of hydromechanical coupling in fractured rock engineering. *Hydrogeology Journal*, *11*(1), 7–40. https://doi.org/10.1007/s10040-002-0241-5

Rutqvist, J., Wu, Y.-S., Tsang, C.-F., & Bodvarsson, G. (2002). A modeling approach for analysis of coupled multiphase fluid flow, heat transfer, and deformation in fractured porous rock. *International Journal of Rock Mechanics and Mining Sciences*, *39*(4), 429–442. https://doi.org/10.1016/s1365-1609(02)00022-9

Salimzadeh, S., Paluszny, A., Nick, H. M., & Zimmerman, R. W. (2018). A three-dimensional coupled thermo-hydro-mechanical model for deformable fractured geothermal systems. *Geothermics*, *71*, 212–224. https://doi.org/10.1016/j.geothermics.2017.09.012

Samuelson, J., Elsworth, D., & Marone, C. (2009). Shear-induced dilatancy of fluid-saturated faults: Experiment and theory. *Journal of Geophysical Research*, *114*, B12404. https://doi.org/10.1029/2008jb006273

Samuelson, J., & Spiers, C. J. (2012). Fault friction and slip stability not affected by CO_2 storage: Evidence from short-term laboratory experiments on North Sea reservoir sandstones and caprocks. *International Journal of Greenhouse Gas Control*, *11*, S78–S90. https://doi.org/10.1016/j.ijggc.2012.09.018

Scanlon, B. R., Mace, R. E., Barrett, M. E., & Smith, B. (2003). Can we simulate regional groundwater flow in a karst system using equivalent porous media models? Case study, Barton Springs Edwards aquifer, USA. *Journal of Hydrology*, *276*(1–4), 137–158. https://doi.org/10.1016/s0022-1694(03)00064-7

Stephanson, O., Jing, L., & Tsang, C. F., (Eds.). (1997). *Coupled thermo-hydro-mechanical processes of fractured media: Mathematical and experimental studies*. Elsevier.

Taron, J., & Elsworth, D. (2009). Thermal-hydrologic-mechanical-chemical processes in the evolution of engineered geothermal reservoirs. *International Journal of Rock Mechanics and Mining Sciences*, *46*(5), 855–864. https://doi.org/10.1016/j.ijrmms.2009.01.007

Thomas, R. N., Paluszny, A., & Zimmerman, R. W. (2020). Permeability of three-dimensional numerically grown geomechanical discrete fracture networks with evolving geometry and mechanical apertures. *Journal of Geophysical Research: Solid Earth*, *125*, e2019JB018899. https://doi.org/10.1029/2019jb018899

Tsang, C.-F. (1999). Linking thermal, hydrological, and mechanical processes in fractured rocks. *Annual Review of Earth and Planetary Sciences*, *27*(1), 359–384. https://doi.org/10.1146/annurev.earth.27.1.359

Vallier, B., Magnenet, V., Schmittbuhl, J., & Fond, C. (2020). THM modeling of gravity anomalies related to deep hydrothermal circulation at Soultz-sous-Forêts (France). *Geothermal Energy*, *8*(1), 1–21. https://doi.org/10.1186/s40517-020-00167-8

Wang, K., & Sun, W. (2018). A multiscale multi-permeability poroplasticity model linked by recursive homogenizations and deep learning. *Computer Methods in Applied Mechanics and Engineering*, *334*, 337–380. https://doi.org/10.1016/j.cma.2018.01.036

Wang, T., Sun, Z., Zhang, K., Jiang, C., Xin, Y., & Mao, Q. (2019). Investigation on heat extraction performance of fractured geothermal reservoir using coupled thermal-hydraulic-mechanical model based on equivalent continuum Method. *Energies*, *12*(1), 127.

Wang, Y., Li, T., Chen, Y., & Ma, G. (2019). A three-dimensional thermo-hydro-mechanical coupled model for enhanced geothermal systems (EGS) embedded with discrete fracture networks. *Computer Methods in Applied Mechanics and Engineering*, *356*, 465–489. https://doi.org/10.1016/j.cma.2019.06.037

Watanabe, N., Wang, W., Taron, J., Görke, U. J., & Kolditz, O. (2012). Lower-dimensional interface elements with local enrichment: Application to coupled hydro-mechanical problems in discretely fractured porous media. *International Journal for Numerical Methods in Engineering*, *90*(8), 1010–1034.

Witherspoon, P. A., Wang, J. S. Y., Iwai, K., & Gale, J. E. (1980). Validity of cubic law for fluid flow in a deformable rock fracture. *Water Resources Research*, *16*(6), 1016–1024. https://doi.org/10.1029/wr016i006p01016

Yao, J., Zhang, X., Sun, Z., Huang, Z., Liu, J., Li, Y., et al. (2018). Numerical simulation of the heat extraction in 3D-EGS with thermal-hydraulic-mechanical coupling method based on discrete fractures model. *Geothermics*, *74*, 19–34. https://doi.org/10.1016/j.geothermics.2017.12.005

Yoshioka, K., Parisio, F., Naumov, D., Lu, R., Kolditz, O., & Nagel, T. (2019). Comparative verification of discrete and smeared numerical approaches for the simulation of hydraulic fracturing. *GEM-International Journal on Geomathematics*, *10*(1), 13. https://doi.org/10.1007/s13137-019-0126-6

Zareidarmiyan, A., Parisio, F., Makhnenko, R., Salarirad, H., & Vilarrasa, V. (2020). *Data for how equivalent are equivalent porous media?* Digital. CSIC. Retrieved from https://digital.csic.es/handle/10261/212935

Zareidarmiyan, A., Salarirad, H., Vilarrasa, V., De Simone, S., & Olivella, S. (2018). Geomechanical response of fractured reservoirs. *Fluids*, *3*(4), 70. https://doi.org/10.3390/fluids3040070

Zareidarmiyan, A., Salarirad, H., Vilarrasa, V., Kim, K.-I., Lee, J., & Min, K.-B. (2020). Comparison of numerical codes for coupled thermo-hydro-mechanical simulations of fractured media. *Journal of Rock Mechanics and Geotechnical Engineering*, *12*(4), 850–865. https://doi.org/10.1016/j.jrmge.2019.12.016

Zhou, J. Q., Chen, Y. F., Tang, H., Wang, L., & Cardenas, M. B. (2019). Disentangling the simultaneous effects of inertial losses and fracture dilation on permeability of pressurized fractured rocks. *Geophysical Research Letters*, *46*(15), 8862–8871. https://doi.org/10.1029/2019gl083355

Zimmerman, R. W., & Bodvarsson, G. S. (1996). Hydraulic conductivity of rock fractures. *Transport in Porous Media*, *23*(1), 1–30. https://doi.org/10.1007/bf00145263